Mon. Not. R. Astron. Soc. **306**, 931–942 (1999)

M4–18: the planetary nebula and its WC10 central star

Orsola De Marco[1,2]★ and Paul A. Crowther[1]

[1]*Department of Physics and Astronomy, University College London, Gower Street, London WC1E 6BT*
[2]*Institute für Astronomie, ETH Zentrum, Scheuchzter-Strasse 7, Zürich CH-8092, Switzerland*

Accepted 1999 February 24. Received 1999 February 22. in original form 1999 January 7

ABSTRACT

We present a detailed analysis of the planetary nebula M4–18 (G146.7+07.6) and its WC10-type Wolf–Rayet (WR) central star, based on high-quality optical spectroscopy (WHT/UES, INT/IDS, WIYN/DensPak) and imaging (*HST*/WFPC2). From a non-LTE model atmosphere analysis of the stellar spectrum, we derive $T_{\rm eff} = 31\,{\rm kK}$, $\log(\dot{M}/{\rm M}_{\odot}\,{\rm yr}^{-1}) = -6.05$, $v_{\infty} = 160\,{\rm km\,s}^{-1}$ and abundance number ratios of ${\rm H/He} < 0.5$, ${\rm C/He} = 0.60$ and ${\rm O/He} = 0.10$. These parameters are remarkably similar to those of He 2–113 ([WC10]). Assuming an identical stellar mass to that determined by De Marco et al. for He 2–113, we obtain a distance of 6.8 kpc to M4–18 [$E(B-V) = 0.55$ mag from nebular and stellar techniques]. This implies that the planetary nebula of M4–18 has a dynamical age of ~3100 yr, in contrast to ≥270 yr for He 2–113. This is supported by the much higher electron density of the latter. These observations may be reconciled with evolutionary predictions only if [WC]-type stars exhibit a range in stellar masses.

Photoionization modelling of M4–18 is carried out using our stellar WR flux distribution, together with blackbody and Kurucz energy distributions obtained from Zanstra analyses. We conclude that the ionizing energy distribution from the WR model provides the best consistency with the observed nebular properties, although discrepancies remain.

Key words: stars: individual: M4–18 – stars: Wolf–Rayet – planetary nebulae: general.

1 INTRODUCTION

Low-excitation Wolf–Rayet (WR) central stars of planetary nebulae (PNe; denoted [WR] following van der Hucht et al. 1981) are thought to represent the beginning of hydrogen-deficient central star evolution, just following the ejection of the PN which occurs at the top of the asymptotic giant branch (AGB). However, discrepancies between observed abundances and those predicted by theory led to the proposal that H-deficient central stars of PNe (CSPNe) are the result of the rebirth of a white dwarf, after a late helium-shell pulse (Iben et al. 1983). Following this interpretation, the search began for characteristics common to PNe with WC nuclei that could be used to distinguish them from those with H-rich central stars, and thus establish that the two classes have followed different evolutions. However, it soon emerged that nebulae associated with [WC] central stars are indistinguishable from those around H-rich CSPNe (Gorny & Stasinska 1995).

To seek a solution to this problem and to determine the evolution of WR-type nuclei, a flurry of empirical and modelling analyses of WC central stars were carried out by several groups (e.g. Leuenhagen, Hamann & Jeffery 1996, hereafter LHJ). The present study focuses on M4–18 (PN G146.7+07.6, IRAS 04215+6000), a PN with a [WC10] central star (following the classification Crowther, De Marco & Barlow 1998a). One may reasonably ask why yet another study of a late WC-type CSPN is necessary. Recent stellar (LHJ) and nebular (Surendiranath & Rao 1995, hereafter SR) models for M4–18 exist in the literature, together with empirical determinations of its PN properties (e.g. Goodrich & Dahari 1985). The justification is that previous studies considered the star and nebula of M4–18 in isolation, making it impossible to relate nebular and stellar results; additionally, a comparison between the nebular properties of M4–18 with other PNe associated with spectroscopically similar stars suggests that [WCL] stars can follow different evolutionary paths; this key aspect has never been given due attention.[1] De Marco, Barlow & Storey (1997) and De Marco & Crowther (1998, hereafter DC) carried out a rigorous analysis of the central stars and PNe of the [WC10] central stars CPD–56°8032 and He 2–113. We follow these methods for M4–18, so that the relative results can be compared with confidence.

Our analysis of M4–18 also extends the photoionization

★ E-mail: od@star.ucl.ac.uk

[1] Pottasch (1996) remarked that the PNe around M4–18 and He2–113 (another [WC10] star) are very different, hinting that the two central stars cannot have followed the same evolutionary path, but nobody took this argument past table 10 of his contribution.

modelling of CPD–56°8032 and He 2–113 by DC using flux distributions appropriate for WR stars. DC identified a major discrepancy between the observed and predicted nebular properties for these PNe; either the lack of heavy-element line blanketing in the wind models was to blame, or the geometry and high nebular densities of those PNe meant that they represented poor probes of the Lyman continuum flux of their central stars. As we shall demonstrate, the PN of M4–18, with a significantly lower electron density, provides a more rigorous test of the theoretical flux distribution.

In Section 2 we will describe the observations, while in Section 3 we will discuss basic observational quantities, including reddening. Section 4 discusses the distance towards M4–18, while a quantitative analysis is carried out in Section 5. Archive *Hubble Space Telescope* (*HST*) images are presented in Section 6, while we carry out a nebular abundance analysis in Section 7. In Section 8 photoionization modelling of the PN is carried out. Finally, we draw our conclusions in Section 9.

2 OBSERVATIONS AND DATA REDUCTION

We have obtained high-quality optical spectroscopy of M4–18 using the 4.2-m William Hershell Telescope (WHT), the 2.5-m Isaac Newton Telescope (INT) and the 3.5-m Wisconsin-Indiana-Yale-NOAO telescope (WIYN). Archival *International Ultraviolet Explorer* (*IUE*) ultraviolet (UV) spectroscopy and *HST* optical imaging of M4–18 were obtained from the Uniform Low-Dispersion Archive (Talavera 1988) at the Rutherford Appleton Laboratory, and the *HST* data archive at the Space Telescope Science Institute, respectively. The *HST* Wide Field and Planetary Camera 2 (WFPC2) data set is discussed further in Section 6.

2.1 Optical spectroscopy

M4–18 was observed at the INT, using the Intermediate Dispersion Spectrograph (IDS), together with the 235-mm camera and a 1024×1024 pixel Tektronix CCD, between 1996 July 17 and 23. Four settings with the 1200B/Y gratings provided complete wavelength coverage in the range 3800–6800 Å, at a spectral resolution of 1.5 Å using a 1.5-arcsec slit. Additional observations with the 300 V grating and an 8-arcsec slit (including the entire nebula) provided an absolute flux calibration at a spectral resolution of 9.5 Å. The data were reduced in a standard manner using the IRAF package, with wavelength calibrations achieved using Cu-Ne and Cu-Ar arc lamps and absolute flux-calibrated data obtained by comparing our wide-slit observations of M4–18 with observations of the Oke (1990) standards B2IV star BD+33°2642 and the Op star BD+28°4211.

High-spectral-resolution ($R \sim 30\,000$) observations of M4–18 were obtained at the WHT using the Utrecht Echelle Spectrograph (UES) in service mode on 1996 November 27. A 1024×1024 pixel Tektronix CCD provided a complete spectral range of 4200–5850 Å; two exposures, each of duration 2400 s, achieved a continuum signal-to-noise ratio of 40. The data were reduced in a standard manner using the IRAF package, with wavelength calibration achieved relative to a comparison Th-Ar arc. For flux calibration, the Oke (1990) standard G191B2b (DA0) was used. Subsequent data reduction was carried out with the DIPSO package (Howarth & Murray 1991).

Additional high-resolution ($R \sim 19\,000$) spectroscopy was obtained on 1998 November 13 by D. Sawyer with the WIYN 3.5-m telescope and the DensPak fibre array, in the range 5770–6010 Å. Three exposures, each lasting 600 s, were obtained with a signal-to-noise ratio of 20. The data were reduced with standard IRAF routines. Wavelength calibration was with respect to a Th-Ar lamp. These spectra allowed us to measure the radial velocity shifts of the interstellar Na I D lines.

Finally, our high-resolution INT and WHT observations were scaled to the continuum level of the wide-slit INT spectra, which were obtained during photometric conditions. By convolving our observed spectrophotometry with suitable synthetic filters (courtesy of J. R. Deacon) we obtained measurements of both wide-band Johnson photometry ($V = 14.11$ and $B = 14.24$ mag) and narrow-band Smith (1968) photometry ($v = 14.14$ and $b = 14.16$ mag). Our measurements are in reasonable agreement with Shaw & Kaler (1985), who obtained a (nebula-corrected) visual brightness of $\sim$14.0 mag.

2.2 Ultraviolet spectroscopy

We utilized four (SWP and LWR/LWP) low-resolution *IUE* large-aperture spectroscopic observations of M4–18 obtained between 1980 August and 1991 August (LWR8401 was not used because it is affected by a cosmic ray hit at the wavelength of the C II] line λ2326; Goodrich & Dahari 1985). Although of poor quality, these provided constraints on the interstellar reddening towards M4–18, and allowed us to obtain estimates of the nebular carbon abundance.

3 BASIC OBSERVATIONAL QUANTITIES

3.1 Radial and nebular expansion velocity

The radial velocity was measured from Gaussian fits to the nebular Balmer lines observed in our optical data sets. WHT–UES observations of Hβ–γ indicated a mean heliocentric radial velocity of $-51.6 \pm 1.0\,\mathrm{km\,s^{-1}}$ (corresponding to an LSR radial velocity of $-50.8 \pm 1.0\,\mathrm{km\,s^{-1}}$). These results are supported by our lower resolution INT observations, which indicate a heliocentric radial velocity of $-46.1 \pm 5.0\,\mathrm{km\,s^{-1}}$.

We used the FWHM of nebular profiles (Hβ, Hγ and λ5755 [N II]) in our WHT–UES observations (FWHM $\sim 6\,\mathrm{km\,s^{-1}}$) to determine the expansion velocity of the PN of M4–18, which was revealed to be $v_{\rm exp} = 19 \pm 0.5\,\mathrm{km\,s^{-1}}$. [The value reported on the ESO PN catalogue (Acker et al. 1992) of $12\,\mathrm{km\,s^{-1}}$ derives from an average of [O III] ($7.5\,\mathrm{km\,s^{-1}}$) and [N II] ($17.0\,\mathrm{km\,s^{-1}}$); we note that it is inappropriate to average values obtained from lines belonging to a mixture of ionization stages, since high-ionization lines may originate from inner, slower parts of the PN.]

3.2 Interstellar reddening

Reddening determinations towards M4–18 from the literature range from $E(B-V) = 0.48$ (SR) to $E(B-V) = 0.90$ (Goodrich & Dahari 1985). We derive interstellar reddenings using observed Balmer line fluxes, which are listed in Table 1. Our wide-slit INT Hβ nebular flux is in reasonable agreement with the determinations of $1.04 \times 10^{-12}\,\mathrm{erg\,cm^{-2}\,s^{-1}}$ by Goodrich & Dahari (1985), and $1.17 \times 10^{-12}\,\mathrm{erg\,cm^{-2}\,s^{-1}}$ by Carrasco, Serrano & Costero (1983, 1984).

We adopt $N_{\rm e} = 10^4\,\mathrm{cm^{-3}}$ and $T_{\rm e} = 10^4$ K (these are revised

Table 1. Balmer fluxes (erg cm^{-2} s^{-1}) measured for the nebular hydrogen lines of M4–18.

Line	WHT–UES narrow slit	INT–IDS narrow slit	INT–IDS wide slit
Hα	–	2.69×10^{-12}	–
Hβ	6.61×10^{-13}	5.75×10^{-13}	8.95×10^{-13}
Hγ	2.30×10^{-13}	–	–

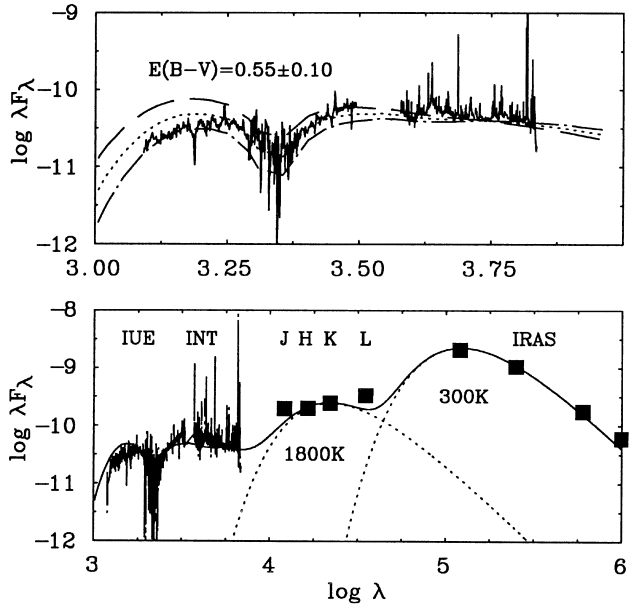

Figure 1. Upper panel: observed ultraviolet and optical spectrophotometry of M4–18 (units are erg cm^{-2} s^{-1}) from *IUE* and INT, together with theoretical energy distributions reddened by $E(B-V) = 0.45$ (dashed), 0.55 (dotted) and 0.65 mag (dot-dashed) using a standard Galactic extinction curve (Seaton 1979; Howarth 1983). Lower panel: as above, except including near- and mid-IR photometry from SR and *IRAS* (filled-in squares), plus a two-component blackbody fit (dotted lines) to the IR excess caused by dust in the PN.

slightly in Section 7), and the Galactic extinction law of Howarth (1983) plus hydrogen recombination coefficients from Storey & Hummer (1995). Unfortunately, Hα is severely blended with [N II] in our wide-slit INT observations, so we have to rely on narrow-slit observations which imply $E(B-V) = 0.45$ mag from Hα–Hβ [WHT Hβ–Hγ observations imply $E(B-V) = 0.61$].

We can also derive a reddening towards M4–18 following Milne & Aller (1975), using our observed Hβ flux, together with the observed 5-GHz flux of 22 mJy from Aaquist & Kwok (1990). This method implies a higher reddening of $E(B-V) = 0.65$ mag.

Therefore extinctions in the range $E(B-V) = 0.45$–0.65 mag are implied from the *nebula*, so we can now test which extinction reproduces the observed UV and optical *stellar* flux distribution, making use of our theoretical energy distribution from Section 5. In Fig. 1 we compare observed UV and optical spectrophotometry of M4–18 with our theoretical model for interstellar extinctions of $E(B-V) = 0.45$, 0.55 and 0.65 mag. We find that 0.55 ± 0.05 mag, provides the best match to observations. [The only previous reddening determination towards M4–18 from spectrophotometry was by LHJ, who obtained $E(B-V) = 0.70$ from a continuum fit to exclusively UV data.] We therefore adopt $E(B-V) = 0.55$ as appropriate to both the nebular and stellar observations of M4–18.

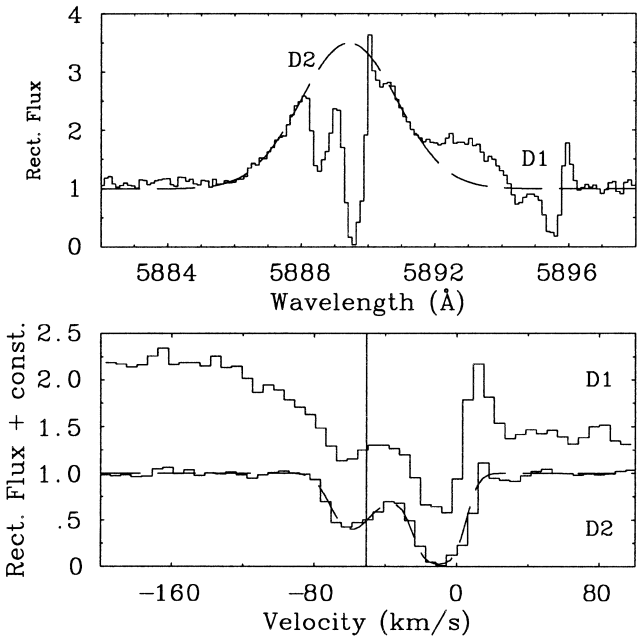

Figure 2. Upper panel: the Na I D lines in the WIYN spectrum of M4–18. The dashed line shows a one-Gaussian fit to the main stellar emission feature. Lower panel: the rectified D2 spectrum in the LSR rest frame, fitted by a three-cloud model (dashed line). D1 is also shown. The vertical line marks the LSR radial velocity of the PN.

Fig. 1 also includes blackbody fits to the infrared (IR) excess of M4–18, representing warm dust from its PN, based on near-IR observations from SR, plus colour-corrected 12–100 μm photometry from *IRAS*. We find that a two-component blackbody fit is necessary, indicating the presence of hot (∼1800 K) and warm (∼300 K) dust. DC found somewhat cooler dust properties for CPD–56°8032 and He 2–113.

4 THE DISTANCE TO M4–18

Distance estimates to M4–18 range from 1 to 7 kpc (Cahn, Kaler & Stanghellini 1992; SR). De Marco, Barlow & Storey (1997) obtained estimates of the distances to CPD–56°8032 and He 2-113 based on the LSR radial velocities of the interstellar Na I D lines, or following the assumption that the entire bolometric luminosity is reradiated in the IR by cool circumstellar dust. The electron density of the PN of M4–18 is more than 10 times lower than that of CPD–56°8032 and He 2-113 (Section 7), with *IRAS* fluxes about 30 times lower, suggesting that the stellar luminosity is unlikely to be entirely reradiated in the infrared.

In Fig. 2 we present the WIYN/DensPak observations in the spectral region 5880–5900 Å, showing the Na I D lines superimposed on a stellar emission blend (C II M5, C III M20 and He II λ5897; De Marco et al. 1997). To determine the radial velocities of the individual Na I D line components, we used a model that calculates absorption profiles for a variety of interstellar clouds with Gaussian line-of-sight velocity distributions (implemented into the ISCALC routine in the DIPSO package). To rectify the Na I D lines, we 'snipped' the D2 absorption and neglected the spectrum longward of ∼5892 Å, thereby approximating the broad emission feature with a single Gaussian (dashed line in the upper panel of Fig. 2).

The three-cloud component fit to the Na I D2 line is presented

Table 2. Parameters of the three-cloud model shown in Fig. 2. The velocity dispersion parameter b is defined in Howarth & Phillips (1986), while N is the Na I column density. The radial velocity (RV) components are in the LSR rest frame, while D is the distance implied by the Brand & Blitz (1993) galactic rotation curve for material near the galactic plane.

Cloud no.	b ($\mathrm{km\,s^{-1}}$)	Log(N/$\mathrm{cm^{-2}}$)	RV ($\mathrm{km\,s^{-1}}$)	D (kpc)
1	13.0	13.0	-60.0 ± 5.0	–
2	20.0	12.8	-37.0 ± 5.0	>1.5
3	12.0	13.6	-10.0 ± 5.0	>1.0

in Fig. 2 (lower panel), with the corresponding parameters listed in Table 2. Although we were unable to carry out the same procedure for D1, it is clear from Fig. 2 that the positions of the D1 absorption line components match those of the D2 components.

If the $-60\,\mathrm{km\,s^{-1}}$ radial velocity component is of interstellar origin, the Galactic radial velocity map of Brand & Blitz (1993) indicates that M4–18 lies beyond 10 kpc. However, at this distance, M4–18 would lie 1.2 kpc above the Galactic plane, where neutral sodium is likely to be scarce (the scaleheight of neutral hydrogen was determined to be 144 ± 80 pc by Shull & Van Steenberg 1985). Moreover, the Brand & Blitz (1993) radial velocity curve was obtained from measurements of H II regions with a scaleheight of only 67 pc. In the direction of M4–18, it can be considered reasonably accurate up to a distance from the Galactic plane of a few times this value (≈200 pc; several measurements of H II regions at ∼400 pc above the Galactic plane exist for this line of sight). Interstellar material in the direction of M4–18 therefore extends to a distance of ∼1.5 kpc, corresponding to a radial velocity of $-30\,\mathrm{km\,s^{-1}}$. Na I D line components with radial velocity more negative than this value are unlikely to be interstellar. Considering the uncertainty on the Galactic rotation curve, we identify the observed $-37\,\mathrm{km\,s^{-1}}$ component to be of interstellar origin. Consequently, Na I D lines simply argue for the distance towards M4-18 being greater than 1.5 kpc.

We attribute the $-60\,\mathrm{km\,s^{-1}}$ component to nebular material. Although we may expect M4–18 not to have a neutral envelope since it is optically thin (see Section 8), Na I was observed in other PNe by Dinerstein, Sneden & Uglum (1995), some of which are also optically thin. If Na I is present in the PN shell, its expansion velocity can be obtained from the difference between the LSR radial velocity of the PN ($-50.8\,\mathrm{km\,s^{-1}}$; Section 3) and the radial velocity shift of the Na I D line component at $-60\,\mathrm{km\,s^{-1}}$. This results in $9\,\mathrm{km\,s^{-1}}$, significantly lower than the ionized shell expansion velocity ($19\,\mathrm{km\,s^{-1}}$). Neutral shells moving considerably slower than the ionized envelopes were detected by Dinerstein, Sneden & Uglum in two other PNe (SwSt 1 and IC3568).

Therefore we follow the alternative approach of DC for CPD–56°8032 and He 2-113 based on assuming a core mass of 0.62 $\mathrm{M_\odot}$ [obtained by X.-W. Liu (private communication) for five LMC WR CSPNe], and applying the helium-burning post-AGB evolutionary tracks of Vassiliadis & Wood (1994) to obtain a stellar luminosity of 5250 $\mathrm{L_\odot}$. Utilizing the observed v-band magnitude for M4–18 from our spectrophotometry, together with the interstellar extinction of $E(B-V) = 0.55 \pm 0.05$ mag and bolometric correction from our WR model (Section 5.2), we obtain a distance of ≈6.8 kpc. This is in excellent agreement with recent statistical distances for M4–18, which range from 6.7 to 7.1 kpc, as summarized by Zhang (1995), and with the distance implied by the $-37\,\mathrm{km\,s^{-1}}$ Na I D line component.

Of course, the masses of all WC central stars need not be identical. From Vassiliadis & Wood (1994) and Blöcker (1995), the possible range in luminosity for a CSPN is ∼2500–16 000 $\mathrm{L_\odot}$, corresponding to a possible range in distance of 4.8–12.0 kpc. Consequently, all distances lower than this minimum are excluded. For example, SR adopted a distance of 1 kpc, based on a relationship between the dust temperature and the PN radius (Pottasch et al. 1984). Using our bolometric correction, an unrealistically low stellar luminosity of 110 $\mathrm{L_\odot}$ would be implied for this distance. (Alternatively, an unrealistically high bolometric correction of −6 mag would be required assuming the luminosity from SR, namely 2500 $\mathrm{L_\odot}$).

In summary, we adopt a distance of 6.8 kpc to M4–18, assuming a mass and luminosity identical to that obtained by DC for He 2–113. However, although M4–18 and He 2–113 are spectroscopically very similar (Section 5), this assumption could be in error. The existence of massive WC stars and CSPNe with very similar spectra, such as He 2–99 ([WC9]) and HD 164270 (WC9) (see Mendez et al. 1991) is a clear indication that spectral similarities do not necessarily indicate similarities in mass. This estimate, on the other hand, is in agreement with the limits imposed by stellar evolution.

5 STELLAR ANALYSIS

In this section we will present our stellar spectrum of M4–18, addressing the important question of whether stellar hydrogen is present. We will also obtain stellar parameters using a sophisticated stellar atmosphere model appropriate for WR stars.

5.1 The stellar spectrum – is hydrogen present?

The stellar spectrum of M4–18 is dominated by emission lines of helium (He I–II), carbon (C II–IV) and oxygen (O II–III). Our high-resolution spectroscopy of M4–18 is presented in Fig. 3 along with a spectrum of the [WC10] central star He 2–113 (from De Marco, Barlow & Storey 1997). It is apparent that their spectral morphologies are remarkably similar, including linewidths, suggesting comparable outflow velocities.

The upper panel of Fig. 4 shows the high-resolution rectified UES spectrum, in the rest frame of the Hβ line. This feature appears to be broadened at its base; additionally, a blueshifted absorption (whose minimum intensity is registered at $185\,\mathrm{km\,s^{-1}}$ to the blue of the line's rest wavelength) is apparent from the rectified spectrum in Fig. 4 (upper panel), suggesting that stellar hydrogen is present in the wind. LHJ determined H/He ratios of <10, 0.64 and <0.5 by number for the [WC10] central stars M4–18, He 2–113 and CPD–56°8032, respectively. De Marco, Barlow & Storey (1997) noticed the same behaviour in the Balmer lines of CPD–56°8032 and He 2–113. However, by comparing these profiles with nebular [O I] lines at 6300 and 6363 Å, they demonstrated that the origin of the broad pedestal under the Hα and Hβ profiles is more likely to be due to an irregular nebular geometry.

For M4–18, nebular [N II] λ5755 and Hγ are also present in the high-resolution UES spectrum, although these are too weak for a comparison to be made. However, we are able to comment on the origin of the P Cygni profile, which cannot be produced by

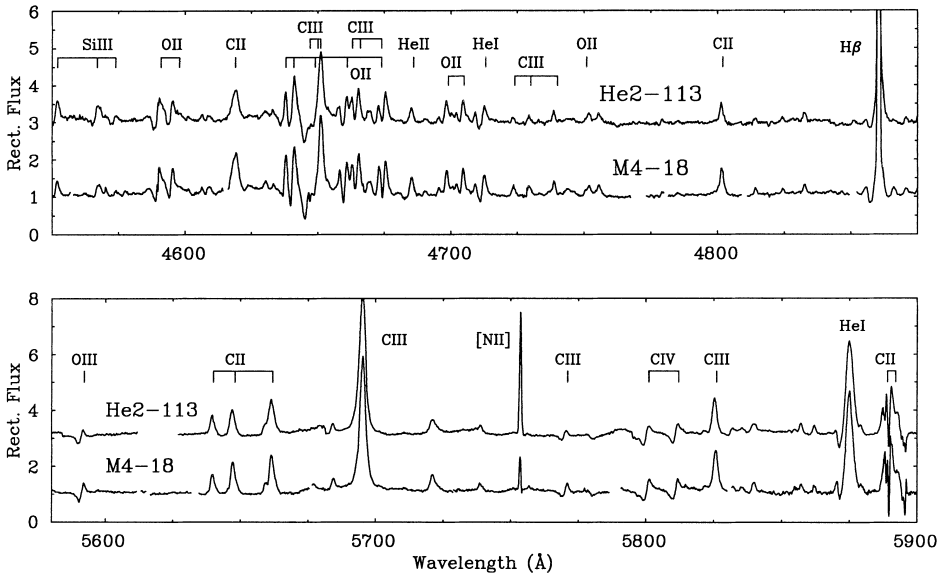

Figure 3. Comparison between rectified spectra of M4–18 (WHT–UES, WIYN–DensPak for $\lambda > 5845$ Å) and He 2–113 (DC), demonstrating the striking similarity in their appearance.

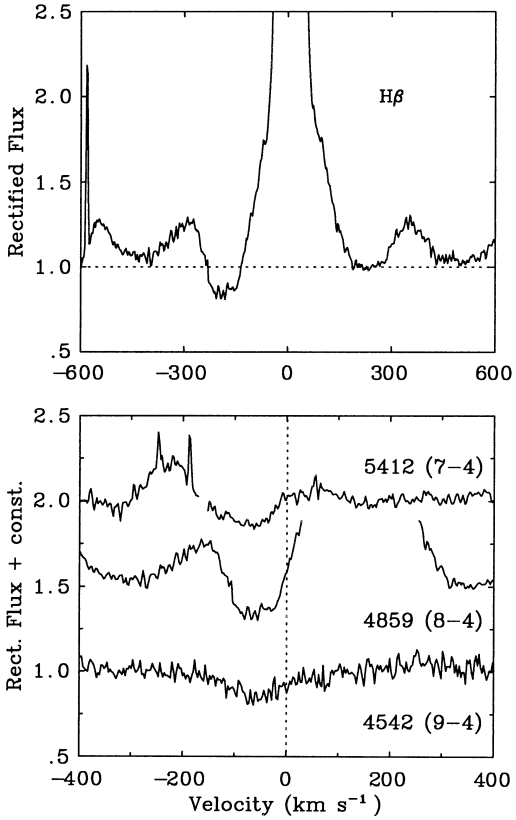

Figure 4. Upper panel: base of the rectified Hβ profile in the WHT–UES data set of M4–18, revealing the presence of (i) broad line wings and (ii) a P Cygni component. Lower panel: comparison of rectified He II Pickering series profiles, indicating that the Hβ P Cygni component is due to He II λ4859 (8–4).

peculiar nebular material. The lower panel of Fig. 4 compares the P Cygni absorption feature in the rest frame of He II 4859.18 Å (transition 8–4), together with the adjacent Pickering members λ4541.46 (9–4) and λ5411.37 (7–4). We find that He II is responsible for this feature.

To summarize, we suspect that Hβ emission wings are solely due to high-velocity components in the *nebular* spectrum, as is the case for the other two [WC10] central stars He 2–113 and CPD–56°8032 (Sahai, Wotten & Clegg 1993; De Marco et al. 1997). To verify this, one would need to observe other nebular lines at high spectral resolution.

5.2 Spectroscopic analysis

Hillier (1987, 1990) theoretical model atmospheres are used in our spectroscopic analysis. These calculations employ an iterative technique to solve the transfer equation in the comoving frame subject to statistical and radiative equilibrium in an expanding, spherically symmetric, homogeneous and steady-state atmosphere. The stellar radius (R_*) is defined as the inner boundary of the model atmosphere, and is located at a Rosseland optical depth of 20. The temperature stratification is determined from the assumption of radiative equilibrium, with the temperature parameter (T_*) defined by the usual Stefan–Boltzmann relation. Similarly, the effective temperature ($T_{\rm eff}$) relates to the radius ($R_{2/3}$) at which the Rosseland optical depth equals 2/3. The spectral synthesis proceeds by fitting line profiles to observed diagnostic He I-II, C II-IV, O II–III lines, together with the absolute visual magnitude. In the absence of high-resolution ultraviolet observations, we measured a stellar wind terminal velocity from optical He I P Cygni profiles, resulting in $160 \pm 15\,{\rm km\,s^{-1}}$.

Fig. 5 presents a comparison of selected observed (WHT–UES) line profiles (solid) with our synthetic spectra (dotted) for M4–18. Overall, the quality of these and other profile fits, covering a wide range in excitation and ionization, is comparable with that achieved for other [WC10] stars by DC, where a more comprehensive explanation of the successes and failures of the model is presented. Overall, the fits also successfully reproduce the strength and shape of many optical emission-line profiles. In particular, the helium spectrum is well fitted, although it is clear from the poor fit to the width of He II λ4686 (Fig. 5, top right panel) that the adopted $\beta = 1$ velocity law is not ideal for this star.

Table 3. Derived stellar parameters of M4–18, including a comparison with LHJ scaled to our assumed luminosity, and demonstrating its very close similarity with He 2–113 (from DC). We include the predicted H I and He I continuum ionizing fluxes (Q_0, Q_1).

Star	Study	V mag	d kpc	$E(B-V)$ mag	T_* kK	R_* $R_\odot$	log L_* $L_\odot$	log $\dot{M}$ $M_\odot\,yr^{-1}$	v_∞ km s^{-1}	H/He	C/He	O/He	log Q_0 s^{-1}	log Q_1 s^{-1}	M_V mag
M4–18	This work	14.1	6.8	0.55	31	2.4	3.72	−6.0	160	<0.5	0.60	0.10	47.2	36.7	−1.8
	LHJ	13.3	3.5	0.70	31	2.3	3.67	−6.0	350	<10	0.40	0.05			−1.6
He 2–113	DC	11.9	1.2	1.00	31	2.5	3.72	−6.1	160	0.0	0.55	0.10	47.2	36.7	−1.8

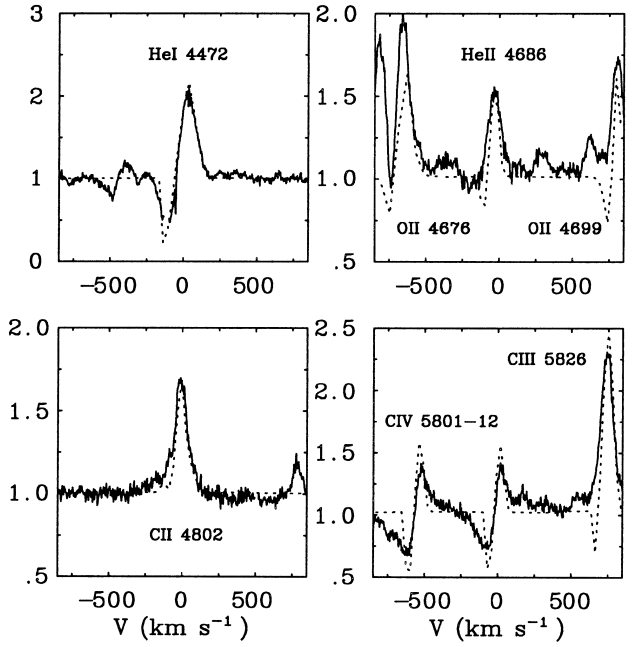

Figure 5. A comparison between selected theoretical profiles for M4–18 (dotted lines) with WHT–UES observations (solid lines). Other profile fits are comparable to those shown for He 2–113 in DC.

P Cygni absorption components are poorly predicted (e.g., C IV $\lambda\lambda$5801–12), further supporting an inadequate velocity structure.

Table 3 presents a summary of our derived stellar parameters. Overall, as reflected in their spectra, the stellar properties and chemistries derived for M4–18 and He 2–113 are almost identical, except for a marginally stronger stellar wind and higher carbon content in the former. For reasons discussed by DC, we consider that derived parameters are not critically dependent on our neglect of heavy-element line blanketing. Although we favour a non-stellar origin for the pedestal at the base of the Hβ line, we have determined a strict upper limit for the stellar hydrogen abundance from fitting the wings of the broad Hβ feature, yielding H/He < 0.5 by number. Our upper limit imposes a tighter constraint on the hydrogen abundance than the analysis of LHJ; this is solely due to the higher spectral resolution of our observations (10 km s^{-1} versus ~150 km s^{-1}).

LHJ included M4–18 in their quantitative study of [WCL] CSPNe. Although their study used an independent code, the same assumptions of spherical symmetry and homogeneity were made. Table 3 also compares our derived stellar parameters with those from LHJ. Overall agreement is very good, although LHJ adopt a higher terminal velocity, again due to the lower resolution of their data set. LHJ derive somewhat lower carbon and oxygen contents for M4–18.

Note that the distance to M4–18 adopted by LHJ is inconsistent with our value, despite deriving an almost identical stellar luminosity. This is because LHJ obtained an extinction of $E(B-V) = 0.7$ mag on the basis of a spectral fit to *exclusively* UV data, inconsistent with our stellar and nebular data sets. Their distance estimate of 3.5 kpc (following Cudworth 1974) then led to a visual continuum magnitude of $v = 13.3$ mag, which our spectrophotometry does not support (Section 3).

6 THE M4–18 NEBULA

We now discuss the PN associated with M4–18, including archive *HST*/WFPC2 narrow-Hα (F656N) images, obtained on 1996 April 18 by R. Sahai. From previous ground-based observations, the PN of M4–18 is known to be extremely small. Radii from optical, mid-IR and radio data sets suggest ≈2 arcsec (Shaw 1985; Zijlstra, Pottasch & Bignell 1989). Although the *HST*/WFPC2 Hα image has recently been presented by Sahai & Trauger (1998), we show it in Fig. 6 in connection with further measurements of its size which are relevant to our analysis. We will abstain, however, from discussing its morphology, which is described in detail by Sahai & Trauger. Fig. 6 shows the nebula both as a grey-scale and a contour map, indicating a clear elongated ring which peaks in intensity at a semimajor axis of 1.28 arcsec (PA = 0°) and a semiminor axis of 0.8 arcsec (PA = 90°). The ring is embedded in a larger, less eccentric shell. From an azimuthal average of the PN, we determine a mean radius of 1.85 ± 0.10 arcsec.

At a distance of 6.8 kpc, the radius of M4–18 corresponds to a physical radius of 0.06 pc (10^4 AU). Using the observed nebular expansion velocity, we obtain a dynamical age of $\tau_{dyn} \sim 3000$ yr. Note that this dynamical age should be reasonable since, as we will show later, the PN is optically thin (Section 8).

7 NEBULAR ABUNDANCE ANALYSIS

Spectroscopy of the M4–18 PN has previously been carried out by Sabbadin (1980), Goodrich & Dahari (1985) and SR. The latter groups combined low-resolution optical and UV spectroscopy to determine PN physical conditions and abundances, while SR also applied their own nebular modelling code. We shall now rederive the electron density and temperature for the PN of M4–18, together with elemental abundances.

7.1 Nebular line fluxes

Our analysis of the PN associated with M4–18 is based on our INT spectrum, in which stellar and nebular features are blended. (Since the nebular diameter is ~3.7 arcsec, ground-based, long-slit spectroscopy does not allow off-star nebular extraction.) We present observed and dereddened line fluxes in Table 4.

The [O II] doublet at 3726 and 3729 Å may be contaminated by a component of the stellar O II M2 triplet λ3727.3. This was judged to be negligible, since the unblended components of this

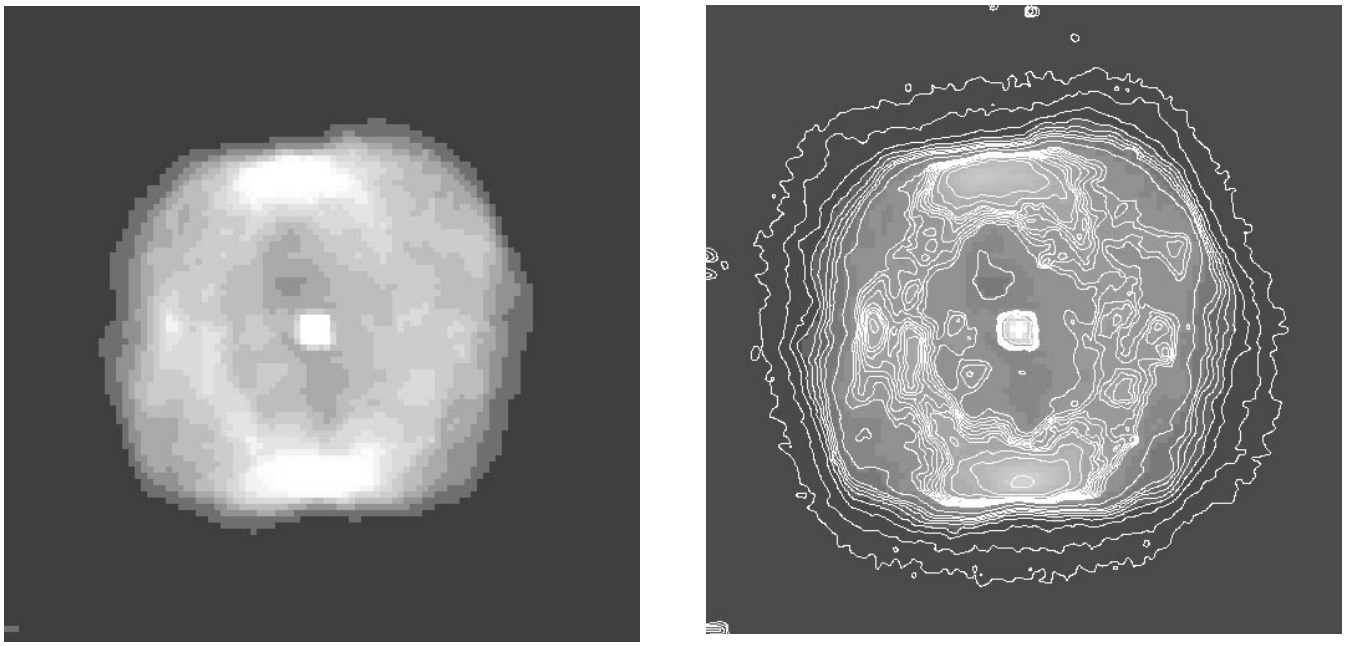

Figure 6. The *HST*/WFPC2 narrow-band Hα (F656N) image of M4–18, shown as a grey-scale plot (left) and a contour plot (right). We present the combined data sets (u35t2401, u35t2402) of R. Sahai, each of 350-s duration. North is towards the top, and east to the left, while the field of view is 4.5×4.5 arcsec^2.

Table 4. Observed (F) and dereddened (I; $E(B-V) = 0.55$ mag) nebular line intensities for M4–18 from our INT/IDS spectrum (*: WHT/UES). The dereddened Hβ flux is 3.62×10^{-12} erg cm^{-2} s^{-1}. Errors are indicated.

Ion	λ (Å)	F (erg cm^{-2} s^{-1})	$100 \times I/\mathrm{I}$ (Hβ)	Errors %
[O II]	3726.0	5.69×10^{-13}	158	30
[O II]	3728.8	3.01×10^{-13}	83.7	30
Hβ	4861.3	5.75×10^{-13}	100	10
[O III]	5006.8*	$\leq 3.6 \times 10^{-15}$	0.06	50
[N II]	5754.6	1.11×10^{-14}	1.35	10
[O I]	6300.3	2.15×10^{-14}	2.2	10
[O I]	6363.8	9.73×10^{-15}	1.0	10
[N II]	6548.0	4.44×10^{-13}	43.1	10
Hα	6562.8	2.69×10^{-12}	260	10
[N II]	6583.4	1.54×10^{-12}	147	20
[S II]	6716.5	7.19×10^{-14}	6.7	10
[S II]	6730.8	1.41×10^{-13}	13.0	20

triplet (at 3712.7 and 3749.5 Å) were weak. However, this doublet was located close to the end of our spectral range, where the sensitivity of the instrument drops sharply. We therefore assign a 30 per cent error to our measurements. Inspection of our UES data set reveals that both the [O III] lines at 5007 and 4959 Å are present,[2] though extremely weak.

Following the approach discussed in De Marco et al. (1997) for the C III] λ1909 line, we consider this to be entirely of stellar origin. Instead, we rely on C II] λ2326 for the determination of the nebular carbon abundance. Its observed equivalent width is 15 ± 4 Å from our dereddened *IUE* spectrum, of which ~4 Å is of stellar origin according to our stellar analysis (Section 5). Since the continuum flux at 2326 Å is in good agreement with our reddened theoretical model distribution (Fig. 1), we are able to obtain a nebular λ2326 flux of 5.34×10^{-12} erg cm^{-2} s^{-1}.

For sulphur, only [S II] $\lambda\lambda$6713,31 lines were available. The [S III] λ3722 line is extremely weak (and blended with [O II] $\lambda\lambda$3726,29), while the $\lambda\lambda$9069,9532 lines were outside our observed spectral range. SR derived the abundance of S^{2+}/H^+, although they derived fluxes for $\lambda\lambda$9069,9532 from indirect techniques. Finally, for nitrogen we used lines at 5755 and 6548 Å, excluding [N II] λ6584 which is blended with the stellar C II line at 6578 Å.

7.2 Nebular temperatures, densities and abundances

We can now proceed to obtaining estimates of the nebular conditions and chemistry. From the usual diagnostic diagram relating Hα/[S II] to [S II] λ6717/λ6731 (see Sabbadin, Minello & Bianchini 1977) we find that M4–18 falls in the photoionization-dominated region, rather than being ionized by shock waves. Therefore the usual nebular diagnostic techniques may be applied here.

We have constructed a nebular diagnostic diagram for M4–18 using [N II], [S II] and [O II] line ratios. These are generated using the RATIO program, written by I. D. Howarth and S. Adams, which solves the equations of statistical equilibrium allowing a determination of N_e as a function of T_e for each ratio. From Fig. 7 we determine $N_e = 10^{3.7 \pm 0.2}$ cm^{-3} and $T_e = 8200 \pm 200$ K for M4–18. The electron density is adopted as a compromise between the [O II] and [S II] doublets. Our results are in reasonable agreement with Sabbadin (1980) and SR, although Goodrich & Dahari (1985) derived a somewhat lower electron temperature ($T_e = 5600 \pm 1600$ K, $N_e = 10^{4.0 \pm 0.1}$ cm^{-3}).

We now utilize our derived nebular parameters to obtain estimates of elemental abundances, which are listed in Table 5.

[2] The [O III] line at 4959 Å is heavily blended with C II stellar components, (i.e., the four components of the dielectronic Multiplet 25), but as we have fitted this spectral region in the spectra of CPD–56°8032 and He 2–113 which did not have any [O III] (De Marco, Storey & Barlow 1998), it was straightforward to recognize its presence.

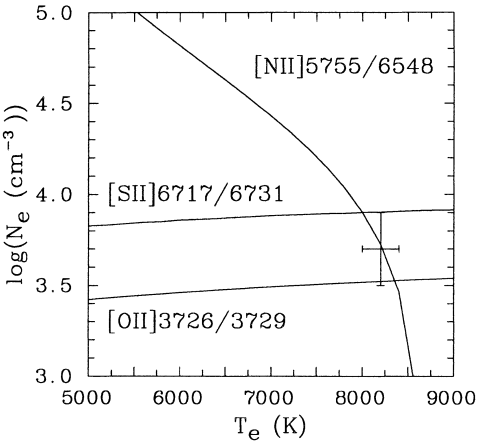

Figure 7. Nebular diagnostic diagram for M4–18.

Table 5. Nebular abundances for M4–18 [on the usual scale where $\log N(\mathrm{H}) = 12.0$]. The C/O number ratio is on a linear scale. The [Ne II] line flux is taken from Aitken & Roche (1982).

Ratio	log(X/H) + 12.0	Diagnostic lines
C	9.08 ± 0.03	C II] λ2326
N	7.60 ± 0.04	[N II] λ5755,λ6548
O	8.62 ± 0.01	[O II] $\lambda\lambda$3726,29
Ne	6.73 ± 0.05	[Ne II] 12.8 μm
S	6.16 ± 0.06	[S II] $\lambda\lambda$6713,31
C/O	2.9 ± 0.6	

For oxygen, nitrogen and carbon we believe the abundances derived from the singly ionized ions to be representative of the whole ionized populations, since [O III] λ5007 and C III] λ1909 are extremely weak or absent. In the case of oxygen, from the upper limit of λ5007 we derive $\mathrm{O}^{2+}/\mathrm{H}^{+} < 4.4 \times 10^{-7}$, corresponding to $\mathrm{O}^{2+}/\mathrm{O}^{+} < 1.0 \times 10^{-3}$.

Equally for sulphur, $\mathrm{S}^{+}/\mathrm{H}^{+}$ should be representative of S/H, since SR obtained $\mathrm{S}^{2+}/\mathrm{S}^{+} \sim 0.1$. Our C/O ratio is much lower than found by De Marco et al. (1997) for CPD–56°8032 and He 2–113, which suggests that the carbon abundance in the PNe of WC central stars is not always higher than average.

Overall, agreement with the abundances obtained by SR is good, except for oxygen [SR derived $\log(\mathrm{O/H}) + 12 = 8.1$] since their dereddened [O II] $\lambda\lambda$3727,29 flux was almost 10 times lower than our measurement. Abundances derived by Goodrich & Dahari (1985) are also in reasonable agreement, once the different reddening and electron properties are taken into account.

8 NEBULAR MODELLING

In this section we derive Zanstra temperatures for M4–18 using blackbody and Kurucz (1991) model atmosphere flux distributions, which are compared to WR flux distribution resulting from the analysis of the CSPN (Section 5). The nebular radial density profile is derived from the *HST* Hα image surface brightness distribution, following the formalism of Harrington & Feibelman (1983). We will carry out photoionization modelling of the PN of M4–18 using all available atmosphere flux distributions, and we will finally compare the modelled parameters with those derived empirically in Section 8.

8.1 Zanstra temperatures

We derive a flux of hydrogen-ionizing photons corresponding to $\log Q_0 = 46.81\,\mathrm{s}^{-1}$ from our Hβ flux (Table 1), dereddened by $E(B-V) = 0.55$ at a distance of 6.8 kpc. We derive a blackbody H I Zanstra temperature of $29\,500 \pm 500$ K, while Kurucz ATLAS9 (Kurucz 1991) model atmospheres yield an effective temperature of $33\,000 \pm 500$ K, using $\log g = 4.0$ models (the minimum gravity tabulated at the required effective temperature). The inferred bolometric luminosities are $4000\,\mathrm{L}_{\odot}$ and $5600\,\mathrm{L}_{\odot}$, respectively. For comparison, Goodrich & Dahari (1985) derived a temperature of 22 000 K using the Stoy (1933) energy-balance method. SR derived a blackbody H I Zanstra temperature of 26 000 K. (They also fitted a blackbody to the optical and UV energy distribution, implying 23 000 K.)

Our WR stellar model for M4–18 predicts $\log Q_0 = 47.23\,\mathrm{s}^{-1}$. This is 2.6 times greater than that inferred from the nebular Hβ flux. In contrast, DC showed how the WR model atmosphere ionizing flux of He 2–113 was 85 times larger than that predicted by Hβ, suggesting that for high-density PNe, gas–dust competition might play a role. Our results for M4–18 confirm their suspicion.

8.2 Nebular surface brightness and density distributions

We have obtained the radial density distribution for M4–18, necessary for photoionization modelling, from the archival *HST*/WFPC2 image (Section 6). For this PN the contribution from nebular continuum emission is negligible.

The azimuthally averaged surface brightness distribution in the Hα image was derived using an algorithm implementation in the SURFPHOT package of MIDAS. The centre of the image was chosen to coincide with the position of the central star. The integrated flux within a radius r was then determined. The central star was contained within a radius of 5 pixels, and the contribution of its continuum flux was subtracted from the nebular flux. The nebular flux, integrated over the entire PN, was then normalized to the dereddened Hβ flux, differentiated with respect to r and divided by $2\pi r$ to obtain the required azimuthally averaged Hβ surface brightness distribution. The result is plotted in Fig. 8 (solid line).

For optically thin PNe, the formalism of Harrington & Feibelman (1983) allows one to derive a density distribution from a surface brightness distribution (see Liu et al. 1995 for an implementation of this method). Photoionization models based on density distributions derived with this formalism, however, tend to give an average density which is too low to reproduce density-sensitive line ratios such as the [O II] λ3726/λ3729 ratio. This deficiency is overcome by introducing a filling factor, ϵ, such that within any small region of material a fraction ϵ is filled with gas, while the complementary fraction $(1-\epsilon)$ is empty. In our case, all density-sensitive line ratios were well reproduced with a filling factor of unity (i.e., a completely filled nebula).

The density distribution which reproduces the Hβ surface brightness distribution, absolute Hβ value and density-sensitive line ratios is shown in Fig. 9 (upper panel). To reproduce the surface brightness shown in Fig. 8, we used $N = 12$ and $K = 1$ in equation (A2) of Harrington & Feibelman (1983). The upper panel of Fig. 9 shows that M4–18 has a central cavity surrounded by a thick shell whose density declines fairly symmetrically as the radius increases.

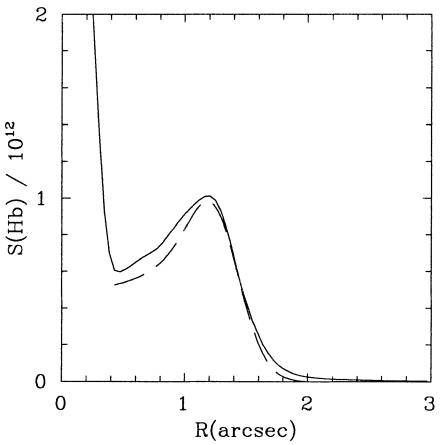

Figure 8. Hβ surface brightness profile (in units of erg cm^{-2} s^{-1} arcsec^{-2}) derived from the *HST* Hα image of M4–18 from an azimuthal average centred on the star (solid line; the central star's continuum is responsible for the intensity peaking near the centre of the nebula). The dashed line is the intrinsic surface brightness distribution predicted by our photoionization model.

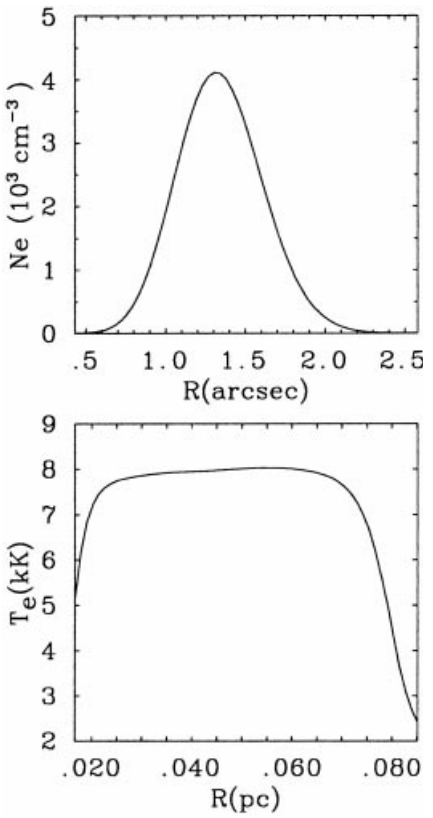

Figure 9. Upper panel: electron density distribution for M4–18 obtained from our analysis of the *HST*/WFPC2 image; Lower panel: electron temperature resulting from our photoionization modelling with the WR flux distribution (assuming a distance of 6.8 kpc).

8.3 The photoionization modelling

The photoionization code used to model M4–18 (Harrington et al. 1982) assumes that the nebula can be represented by a hollow, spherical shell which is ionized and heated solely by the radiation of the central star. This shell is sampled by a network of grid points at each of which the density is supplied. We used 60 grid points and the electron density derived from the Hβ surface brightness (Section 8.2).

Once a distance is adopted, and the dereddened V magnitude of the central star established, the effective temperature of the central star (from the WR stellar analysis or derived by a Zanstra analysis as described in Section 8.1) determines all the other stellar parameters. These parameters are listed in the first three rows of Table 6. The inner nebular radius was fixed at the value derived from the *HST*/WFPC2 observations, scaled to the adopted distance. Elemental abundances are initially set at empirical values, and later adjusted to fit the observed line fluxes if necessary.

Final photoionization models for each flux distribution are compared to observation in Table 6. Overall, very good agreement is reached between observations and model calculations for all diagnostic line ratios (O II, N II and S II) as well as absolute line fluxes. This is an indication of the success of our density distribution, recalling the discrepancy between different diagnostics in Fig. 7.

It is apparent that the WR and Kurucz (1991) stellar flux distributions perform better than the blackbody. Overall, the WR stellar atmosphere is most appropriate to reproduce the line intensities, in spite of the other distributions resulting from Zanstra nebular analyses. In Fig. 9 we present the predicted electron temperature as a function of radius for our WR model. Hydrogen is completely ionized throughout, as is appropriate for an optically thin PN, with a predicted nebular mass of 0.08 M$_\odot$.

A major failure of each model flux distribution is the overestimate of the sulphur ionization balance, and consequent underestimate of the [S II] 6717,31-Å line strengths. (The ratio S^{2+}/S^{+} was estimated to be 0.1 by SR, although a value of <1 is probably more secure.) The poor reproduction of the sulphur ionization balance can be appreciated by inspecting the shape of the ionizing flux distributions in Fig. 10. Metal line blanketing in our WR model atmospheres may help to solve the sulphur problem by reducing the hard UV flux (for the effect of blanketing in late-type WR stars, see Crowther, Bohannan & Pasquali 1998b).

In the case of the oxygen ionization balance, only the WR model predicts the appropriate ratio, with Kurucz (1991) and blackbody atmospheres overestimating the strength of [O III] λ5007. This is illustrated in Fig. 10, where only the WR energy distribution has negligible zero flux below the He I edge at λ504.

Our study supersedes the photoionization modelling of M4–18 by SR. They adopted a distance of 0.9 kpc, and a 22 000-K blackbody, implying a luminosity of 134 L$_\odot$ for the central star. As discussed in Section 4, these quantities are inconsistent with theoretical predictions for CSPNe. Note also that SR also adopted a constant electron density of 6620 cm^{-3}, implying $T_e = 6600$ K (their empirical value was 8500 K).

9 DISCUSSION

We have derived consistent stellar and nebular parameters for the [WC10] central star M4–18 and its PN. Although stellar and nebular analyses have previously been carried out (SR; LHJ), such studies revealed inconsistent parameters (e.g., LHJ disregarded its visual magnitude, while SR adopted an unrealistically low luminosity).

Table 6. Comparison of results from photoionization models for M4–18 with observations [$I(H\beta) = 100$], using WR non-LTE, blackbody and Kurucz (1991) plane-parallel energy distributions. Elemental abundances are by number. Filling factors of $\epsilon = 1$ are assumed throughout.

Parameter	Empirical	WR	Blackbody	Kurucz
$T_{\rm eff}$ (kK)	–	31.0	29.5	33.0
$\log(L_*/L_\odot)$		3.72	3.60	3.75
$\log Q_0$ (s^{-1})	46.81	47.23	46.81	46.81
$N_e(r)$ (cm^{-3})		See Fig. 9 (upper panel)		
He/H	–	0.1	0.1	0.1
C/H $\times 10^3$	1.2	1.2	1.2	1.2
N/H $\times 10^5$	4.0	4.8	5.5	4.0
O/H $\times 10^4$	4.2	4.2	4.2	4.2
Ne/H $\times 10^5$	5.0	4.1	4.1	4.0
S/H $\times 10^6$	1.4	1.4	1.4	1.4
[O II]λ3726/λ3729	1.88	1.82	1.85	1.80
[S II]λ6716/λ6731	0.52	0.60	0.60	0.62
[N II]λ5755/λ6548	0.032	0.027	0.029	0.032
C III] λ1909	0	0.0	11	2.6
C II] λ2326	148	128	96	197
[O II] λ3726	158	155	154	213
[O II] λ3729	84	85	83	118
[O III] λ5007	0	0.0	39	1.0
[N II] λ5755	1.4	1.13	1.14	1.35
[O I] λ6300	2.2	0.049	0.067	0.23
[O I] λ6363	1.0	0.016	0.022	0.075
[N II] λ6548	43	42	41	42
[S II] λ6717	6.7	0.64	0.87	1.29
[S II] λ6731	13	1.73	1.85	2.08
[Ne II] 12.8 μm	32	32	32	32
S^{2+}/S^+	<1	12	15	17
O^{2+}/O^+	$<1.0\times10^{-3}$	∼0	77×10^{-3}	1.6×10^{-3}
$T_e(N^+)$ (K)	8200	7900	8000	8400
τ(H I)	–	1.1	1.6	4.2

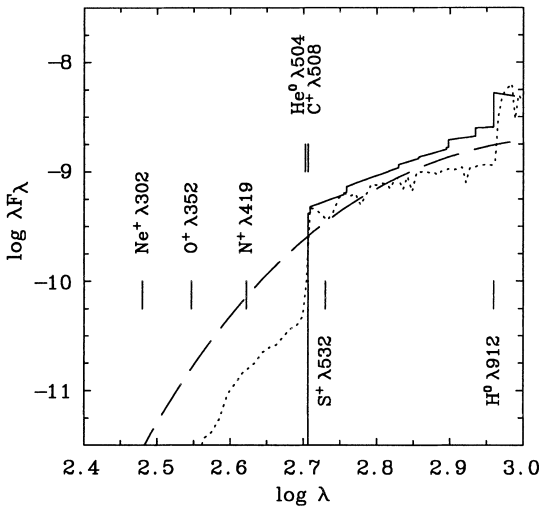

Figure 10. Comparison of Lyman ionizing flux distribution obtained from our stellar analysis of M4–18 (Wolf–Rayet, solid), with black-body (dashed) and Kurucz (1991, dotted) distributions obtained from our nebular Zanstra analysis. Clearly, the WR distribution differs dramatically from the other distributions shortward of the He I edge at λ504, especially at the O II edge at λ353.

While the stellar parameters of M4–18 are almost identical to those of He 2–113, their PNe differ greatly. For M4–18, a dynamical age of 3100 yr is implied for a distance of 6.8 kpc, while the well-determined distance to He 2–113 (De Marco et al. 1997) implies a dynamical age for this PN of ≈270 yr. Since He 2–113 is optically thick, its dynamical age is probably only a lower limit, although there can be little doubt that the PN of He 2–113 is younger, when we consider the respective optical depths and electron densities. How can such spectroscopically similar CSPN have such different PN ages? This difference is hard to reconcile, if M4–18 and He 2–113 have similar masses.

Table 7. Summary of stellar and nebular parameters for M4–18, compared with those for its spectroscopic twin He 2–113 (De Marco et al. 1997; DC). Evolutionary time-scales ($\tau_{\rm evol}$) are from Vassiliadis & Wood (1994) and Blöcker (1995).

D kpc	N_e cm^{-3}	$v_{\rm exp}$ $km\,s^{-1}$	Radius 10^{-3} pc	$\tau_{\rm dyn}$ yr	L_* $L_\odot$	M $M_\odot$	$\tau_{\rm evol}$ yr
			M4–18				
4.8	3300	19	43	2200	2600	0.52	8000
6.8	3300	19	61	3100	5250	0.62	500
12	3300	19	111	5600	16 000	0.84	150
			He 2–113				
1.2	63 000	21	6	≥270	5250	0.62	500

Were we to relax our assumption that all [WC]-type stars have an identical mass, distances in the range 4.2–12 kpc are consistent with our spectrophotometry and the luminosity from theoretical helium-burning tracks. Table 7 shows the properties of M4–18 for this range of distances compared to those of He 2–113 (De Marco et al. 1997; DC). We include the ages predicted by the evolutionary tracks of Blöcker (1995) and Vassiliadis & Wood (1994). (Note that these agree well where comparisons may be carried out.) Ages are predicted to be extremely sensitive to core mass. From figs 15 and 16 of Blöcker (1995), a helium-burning central star of mass 0.52 $M_\odot$ reaches 30 000 K in 8000 yr, while a star of 0.84 $M_\odot$ takes only 150 yr.

Comparisons between dynamical and evolutionary ages should be treated qualitatively (both dynamical and evolutionary ages of the PNe are subject to large uncertainties). Nevertheless, assuming a lower mass for M4–18 than He 2–113 resolves the differences in their PNe. In addition, it resolves the discrepancy between the dynamical and evolutionary ages of M4–18. For a mass of $\sim 0.55\,M_{\odot}$, the dynamical and evolutionary time-scales are both ~ 2500 yr (corresponding to a distance of 5.5 kpc).[3] We note that for He 2–113 the comparison between dynamical and evolutionary time-scales is reasonable if we take into consideration the fact that the dynamical time-scale is merely a lower limit.

If the masses of M4–18 and He 2–113 are different, then masses of WR central stars may span the whole range of possible post-AGB masses, opening the possibility that WR central stars follow a variety of evolutionary paths. It has been suggested (e.g. Rao 1987; SR) that [WC10] central stars are approaching the AGB in a born-again-type evolution (Iben et al. 1983). This claim was based on the apparent inverse correlation between PN diameters and CSPN temperatures. Incorporating the results from DC, this is no longer established. Consequently, there is no evidence that [WC10] CSPN are approaching the AGB. However, our comparison provides evidence that WC central stars are not a homogeneous group, with a range of masses and individual evolutionary patterns. It remains to be confirmed whether WC-type stars can result from a 'born-again' evolution, although the potentially related stars Abell 30 and 78 are associated with well-established born-again PNe (Jacoby & Ford 1983).

ACKNOWLEDGMENTS

We thank John Hillier for kindly providing us with his atmospheric code, and greatly appreciate discussions with Mike Barlow. John Deacon is thanked for providing filter profiles and calibrations. Dave Sawyer of the National Optical Astronomy Observatories is gratefully acknowledged for providing the WIYN/DensPak spectrum of the Na I D lines. OD acknowledges financial support from the Perren Fund during the period of her PhD and the Swiss Research Council jointly with the Institute of Astronomy at the ETH–Zürich for the time and resources used in the final stages of this research. PAC gratefully acknowledges financial support from PPARC and the Royal Society.

The WHT and INT are operated on the island of La Palma by the Isaac Newton Group in the Spanish Observatorio del Roque de los Muchachos of the Instituto de Astrofisica de Canarias. We particularly thank Don Pollacco for obtaining the WHT/UES spectrum as part of a service programme. This research has made use of observations made with the NASA/ESA *Hubble Space Telescope*, obtained from the data archive at the Space Telescope Science Institute, which is operated by the Association of Universities for Research in Astronomy, Inc. under the NASA contract NAS5-26555. IRAF was written and supported by NOAO. MIDAS is developed and distributed by the European Southern Observatory. Calculations have been performed at the CRAY J90 of the RAL Atlas centre, and at the UCL node of the UK Starlink facility.

[3] At a distance of 5.5 kpc, the luminosity, radius and mass-loss rate for M4–18 would be revised to $\log(L_*/L_{\odot}) \sim 3.45$, $R_* = 1.8\,R_{\odot}$ and $\log(\dot{M}/M_{\odot}\,\mathrm{yr}^{-1}) = -6.26$, with other stellar properties unchanged.

REFERENCES

Aaquist O. B., Kwok S., 1990, A&AS, 84, 229
Acker A., Ochsenbein F., Stenholm B., Tylenda R., Marcout J., Schohn C., 1992, Strasbourg–ESO Catalogue of Galactic Planetary Nebulae. ESO, Munich
Aitken D. K., Roche P. F., 1982, MNRAS, 200, 217
Blöcker T., 1995, A&A, 299, 755
Brand J., Blitz L., 1993, A&A, 275, 67
Cahn J. H., Kaler J. B., Stanghellini L., 1992, A&AS, 94, 399
Carrasco L., Serrano A., Costero R., 1983, Rev. Mex. Astron. Astrofis., 8, 187
Carrasco L., Serrano A., Costero R., 1984, Rev. Mex. Astron. Astrofis., 9, 111
Crowther P. A., De Marco O., Barlow M. J., 1998a, MNRAS, 296, 367
Crowther P. A., Bohannan B., Pasquali A., 1998b, in Howarth I. D., ed., ASP Conf. Ser. Vol. 131, Boulder-Munich II: Properties of Hot, Luminous Stars. Astron. Soc. Pac., San Francisco, p. 38
Cudworth K. M., 1974, AJ, 79, 1384
De Marco O., Crowther P. A., 1998, MNRAS, 296, 419 (DC)
De Marco O., Barlow M. J., Storey P. J., 1997, MNRAS, 292, 86
De Marco O., Storey P. J., Barlow M. J., 1998, MNRAS, 297, 999
Dinerstein H. L., Sneden C., Uglum J., 1995, ApJ, 447, 262
Goodrich R. W., Dahari O., 1985, ApJ, 289, 342
Gorny S. K., Stasinska G., 1995, A&A, 303, 893
Harrington J. P., Feibelman W. A., 1983, ApJ, 265, 258
Harrington J. P., Seaton M. J., Adams S., Lutz J. H., 1982, MNRAS, 199, 517
Hillier D. J., 1987, ApJS, 63, 947
Hillier D. J., 1990, A&A, 231, 111
Howarth I. D., 1983, MNRAS, 203, 301
Howarth I. D., Murray J., 1991, Rutherford Appleton Laboratory, Starlink User Note, 50.13
Howarth I. D., Phillips A. P., 1986, MNRAS, 222, 809
Iben I. Jr, Kaler J. B., Truran J. W., Renzini A., 1983, ApJ, 264, 605
Jacoby G., Ford H., 1983, ApJ, 266, 298
Kurucz R. L., 1991, in Philips A. G. D., Upgren A. R., James K. A., eds, Precision Photometry: Astrophysics of the Galaxy. L. Davis Press, Schenectady, p. 27
Leuenhagen U., Hamann W.-R., Jeffery C. S., 1996, A&A, 312, 167 (LHJ)
Liu X. W., Barlow M. J., Blades J. C., Osmer S., Clegg R. E. S., 1995, MNRAS, 276, 167
Mendez R. H., Herrero A., Manchado A., Kudritzki R. P., 1991, A&A, 252, 265
Milne D. K., Aller L. H., 1975, A&A, 38, 183
Oke J. B., 1990, AJ, 99, 1621
Pottasch S. R., 1996, Ap&SS, 238, 17
Pottasch S. R. et al., 1984, A&A, 138, 10
Rao N. K., 1987, QJRAS, 28, 261
Sabbadin F., 1980, A&A, 84, 216
Sabbadin F., Minello S., Bianchini A., 1977, A&A, 60, 147
Sahai R., Trauger J. T., 1998, AJ, 116, 135
Sahai R., Wotten A., Clegg R. E. S., 1993 in Weinberger R., Acker A., eds, Proc. IAU Symp. 155, Planetary Nebulae. Kluwer, Dordrecht, p. 229
Seaton M. J., 1979, MNRAS, 187, 73P
Shaw R. A., 1985, PhD thesis, Univ. Illinois at Urbana-Champaign
Shaw R. A., Kaler J. B., 1985, ApJ, 295, 537
Shull J. M., Van Steenberg M. E., 1985, ApJ, 294, 559
Smith L. F., 1968, MNRAS, 140, 409
Storey P. J., Hummer D. G., 1995, MNRAS, 272, 41
Stoy R. H., 1933, MNRAS, 93, 588

Surendiranath R., Rao N. K., 1995, MNRAS, 275, 685 (SR)
Talavera, A., 1988, ULDA Users Guide, ESA IUE Observatory
van der Hucht K. A., Conti P. S., Lundström I., Stenholm B., 1981, Rev., Space Sci., 28, 227
Vassiliadis E., Wood P. R., 1994, ApJS, 92, 125
Zhang C. Y., 1995, ApJS, 98, 650
Zijlstra A. A., Pottasch S. R., Bignell C., 1989, A&AS, 79, 329

This paper has been typeset from a TEX/LATEX file prepared by the author.